

Quantum and quasiclassical dynamics of C($^{3} P$)+ H$_{2}(^{1} \varSigma_{\text{g}}^+)\rightarrow H(^{2} S)$ + CH($^{2} \varPi$) reaction: Coriolis coupling effects and stereodynamics

Dong Liu(刘栋), Lulu Zhang(张路路), Juan Zhao(赵娟), Qin Zhang(张芹), Yuzhi Song(宋玉志), and Qingtian Meng(孟庆田)

Citation: Chin. Phys. B, 2022, 31 (**4**): 043102. DOI: 10.1088/1674-1056/ac3989
Journal homepage: http://cpb.iphy.ac.cn; http://iopscience.iop.org/cpb

What follows is a list of articles you may be interested in

State-to-state dynamics of reactions H+DH'(v = 0,j = 0) → HH'(v',j')+D/HD(v',j')+H' with time-dependent quantum wave packet method

Juan Zhao(赵娟), Da-Guang Yue(岳大光), Lu-Lu Zhang(张路路), Shang Gao(高尚), Zhong-Bo Liu(刘中波), and Qing-Tian Meng(孟庆田)
Chin. Phys. B, 2021, 30 (**7**): 073102. DOI: 10.1088/1674-1056/abf559

Reaction mechanism of D+ND→N+D_2 and its state-to-state quantum dynamics

Ting Xu(许婷), Juan Zhao(赵娟), Xian-Long Wang(王宪龙), Qing-Tian Meng(孟庆田)
Chin. Phys. B, 2019, 28 (**2**): 023102. DOI: 10.1088/1674-1056/28/2/023102

Novel potential energy surface-based quantum dynamics of ion-molecule reaction $O^{+}+D_2$ →OD^{+}+D

Xian-Long Wang(王宪龙), Feng Gao(高峰), Shou-Bao Gao(高守宝), Lu-Lu Zhang(张路路), Yu-Zhi Song(宋玉志), Qing-Tian Meng(孟庆田)
Chin. Phys. B, 2018, 27 (**4**): 043104. DOI: 10.1088/1674-1056/27/4/043104

State-to-state dynamics of F(^{2}P)+HO(^{2}Π) →O(^{3}P)+HF($^{1}\sum^{+}$) reaction on 1^{3}A" potential energy surface

Juan Zhao(赵娟), Hui Wu(吴慧), Hai-Bo Sun(孙海波), Li-Fei Wang(王立飞)
Chin. Phys. B, 2018, 27 (**2**): 023102. DOI: 10.1088/1674-1056/27/2/023102

State-to-state quantum dynamics of N(^{2}D)+HD (v=0, j=0) reaction

Yong Zhang(张勇)
Chin. Phys. B, 2016, 25 (**12**): 123104. DOI: 10.1088/1674-1056/25/12/123104

Quantum and quasiclassical dynamics of $C(^3P)+H_2(^1\Sigma_g^+) \rightarrow H(^2S) + CH(^2\Pi)$ reaction: Coriolis coupling effects and stereodynamics

Dong Liu(刘栋)[1], Lulu Zhang(张路路)[1,†], Juan Zhao(赵娟)[1], Qin Zhang(张芹)[1], Yuzhi Song(宋玉志)[2], and Qingtian Meng(孟庆田)[2,‡]

[1] *School of Science, Shandong Jiaotong University, Jinan* 250357, *China*
[2] *School of Physics and Electronics, Shandong Normal University, Jinan* 250358, *China*

(Received 14 October 2021; revised manuscript received 11 November 2021; accepted manuscript online 15 November 2021)

The dynamics of $C + H_2 \rightarrow H + CH$ reaction is theoretically studied using the quasiclassical trajectory and quantum mechanical wave packet methods. The analysis of reaction probabilities, integral cross sections, and rate coefficients reveal the essential Coriolis coupling effects in the quantum mechanical wave packet calculations. The calculated polarization-dependent differential cross section, $P(\theta_r)$ and $P(\phi_r)$ show that the $\boldsymbol{j}'$ of product rotational angular momentum is not only aligned along the y axis and the direction of the vector $\boldsymbol{x}+\boldsymbol{z}$, but also strongly oriented along the positive y axis.

Keywords: quantum dynamics, quasiclassical trajectory method, $C + H_2$

PACS: 31.15.xv, 34.10.+x, 03.67.Lx **DOI:** 10.1088/1674-1056/ac3989

1. Introduction

The reactions containing neutral carbon atom play a significant part in the astrophysics of interstellar medium and combustion chemistry.[1–3] As the simplest carbon-containing reaction, $C + H_2$ is important in atmospheric and hydrocarbon combustion. So far, a lot experimentalists[4–9] and theoreticians[10–24] focus on this reaction, its reverse reaction, and potential energy surface (PES).

The reactions of $C(^1D) + H_2(^1\Sigma_g^+)$ based on the singlet states of methylene molecule have been extensively explored, but the investigations about the $C(^3P) + H_2(^1\Sigma_g^+) \rightarrow H(^2S) + CH(^2\Pi)$ reaction based on the triplet electronic ground state of $CH_2(\tilde{X}\,^3A'')$ are limited. In order to study $C(^1D) + H_2(^1\Sigma_g^+)$ reactions, Bussery–Honvault team respectively constructed the full dimensional and adiabatic PESs of CH_2 for the first $1^1A'$ (BHL PES)[20] and second $1^1A''$ (BJHL PES)[21] singlet states using 1748 and 4644 *ab initio* points. Then Bañares and co-authors[25] rebuilt the $1^1A'$ state PES based on the same 1748 *ab initio* points employing the reproducing kernel Hilbert space (RKHS) interpolation method. Their dynamic results are consistent with those obtained on the BHL PES. Based on the BHL PES, Lu *et al.*[26] studied the scalar and vector properties of $H(^2S) + CH(^2\Pi) \rightarrow C(^1D) + H_2(^1\Sigma_g^+)$ reaction applying the quasiclassical trajectory (QCT) and time-dependent wave-packet (TDWP) methods. Lin and Guo[27,28] calculated the probabilities, integral cross sections (ICSs), and rate coefficients using the Chebyshev wave packet method based on RKHS PES. Soon after, another $1^1A'$ PES was constructed by Joseph and Varandas[11] employing double many-body expansion (DMBE) formula and about 2500 *ab initio* points. They further investigated CD/CH branching ratio and isotope effect on the $C(^1D) + H_2(^1\Sigma_g^+)$ reaction with QCT method. Different from the previous $1^1A'$ PES, the PES (called ZMB-a PES) fitted by Zhang and co-workers[29] can accurately describe the regions around conical intersections (CIs) and of van der Waals (vdW) interactions. Due to the differences of the PESs in the regions around the CIs and vdW complexes, Wu *et al.*[30] found that at low collision energies, the values of ICS are much bigger than the previous QCT. Afterwards, based on ZMB-a PES, a lot of dynamic calculations have been done.[31–35]

Concerning the $C(^3P) + H_2(^1\Sigma_g^+) \rightarrow H(^2S) + CH(^2\Pi)$ reaction, its dynamical calculation needs a full-dimensional PES of $CH_2(\tilde{X}\,^3A'')$. In 1993, Harding *et al.*[17] fitted an accurate three-dimensional (3D) PES of triplet electronic state of CH_2 by employing multireference configuration interaction (MRCI) method. This PES can well describe the conical intersections including C_{2v} geometries between the $^3B_1$ and $^3A_2$ states and linear geometries between the $^3\Pi$ and $^3\Sigma^-$ states. Then the rate constant of $H(^2S) + CH(^2\Pi) \rightarrow C(^3P) + H_2(^1\Sigma_g^+)$ reaction was calculated in their work. Based on this PES, Harrevelt *et al.*[36] explicated minor quantum effects in the $CH(^2\Pi) + H(^2S) \rightarrow C(^3P) + H_2(^1\Sigma_g^+)$ reaction by testing calculated reaction probabilities, which illustrates the QCT method can supply realistic estimates of ICSs and the rate constants. Lately, the dynamics of $H(^2S) + CH(^2\Pi) \rightarrow C(^3P) + H_2(^1\Sigma_g^+)/H(^2S) + CH(^2\Pi)$ reactions were explored

†Corresponding author. E-mail: zhanglulu@sdjtu.edu.cn
‡Corresponding author. E-mail: qtmeng@sdnu.edu.cn

© 2022 Chinese Physical Society and IOP Publishing Ltd

in depth by Gamallo *et al.*[23] with quantum mechanical (QM) method. In their work, by analysis of the correlation diagram of the CH_2 electronic states $\tilde{X}\,^3A''$, $\tilde{A}\,^3A''$, $\tilde{a}\,^1A'$, and $\tilde{b}\,^1A''$, and by test of the Renner–Teller and spin–orbit nonadiabatic calculations on $\tilde{X}\,^3A''$, $\tilde{a}\,^1A'$, and $\tilde{b}\,^1A''$, they found that the $H(^2S)+CH(^2\Pi)$ reactions occur essentially on the uncoupled $\tilde{X}\,^3A''$ ground surface. Recently, our team also fitted the $CH_2(\tilde{X}\,^3A'')$ PES,[24] and based on it the probabilities, ICSs, and rate coefficients were calculated, which are in good agreement with other theoretical results. Subsequently, the reaction mechanism, vibrational excitation, and isotope effects on the $H(^2S)+CH(^2\Pi)$ reaction were analyzed in detail by our group[37] using the QCT method.

The present work is to explore the dynamics of the $C(^3P)+H_2(^1\Sigma_g^+)\rightarrow H(^2S)+CH(^2\Pi)$ reaction based on recent $CH_2(\tilde{X}\,^3A'')$ PES[24] according to QM and QCT methods. The schematic representation of the reaction energy profile of the PES is depicted in Fig. 1(a). This panel reflected the title reaction with an endothermic of 1.109 eV, and existence of a deep well with 3.467 eV.

The rest of this paper is organized as follows: In Section 2, we briefly describe the method including QM and QCT calculations. In Section 3, we discuss the Coriolis coupling effects on the title reaction and analyze its stereodynamics. Finally, the conclusions are summarized in Section 4.

2. Methods

2.1. QM calculations

The QM TDWP method is employed to numerically solve the time-dependent nuclear Schrödinger equation using the second-order split-operator scheme, referred to the relevant articles.[38–43] In calculations, the Hamiltonian is expressed in the reactant Jacobi coordinates. Convergence tests are carried out with the total reaction probability for $J=0$ and the optimal numerical parameters are as follows. In the reactant Jacobi coordinates, the R coordinate is set in the range of 0.1 a.u.–30.0 a.u. and the diatomic vibrational coordinate is set to be 0.5 a.u.–25.0 a.u. The number of translational and vibrational basis functions is 300 and 210, respectively. The total propagation time is 6×10^4 a.u. with the time step being 10 a.u. All calculations are performed using both centrifugal sudden (CS) approximation and coupled-channel (CC, including the Coriolis coupling) with $K=5$ used in the CC calculations.

2.2. QCT calculations

Figure 1(b) describes the angle relationship between the initial relative velocity and the final relative velocity vectors in the center-of-mass reference frame, which can be well understood as product rotational polarizations.[44–48] $\boldsymbol{k}$ and $\boldsymbol{k}'$ respectively denote the relative velocity vectors of reactant and product in x–z plane, and they are connected by the angle θ_t. $\boldsymbol{j}'$ is the product rotational angular momentum, and θ_r and ϕ_r are the dihedral and the azimuthal angles of it respectively. The distribution function $P(\theta_r)$ describes the $\boldsymbol{k}$–$\boldsymbol{j}'$ correlation with $\boldsymbol{j}'\cdot k=\cos\theta_r$, expanded in a series of Legendre polynomials,

$$P(\theta_r)=\frac{1}{2}\sum_k(2k+1)a_0^{(k)}p_k(\cos\theta_r), \tag{1}$$

in which the expanding coefficients $a_0^{(k)}$, described by $a_0^{(k)}=\int_0^\pi P(\theta_r)p_k(\cos\theta_r)\sin\theta_r\,\mathrm{d}\theta_r=\langle p_k(\cos\theta_r)\rangle$, are orientation parameter (k is odd) or alignment parameter (k is even), and k is the integer to ensure the convergent results of $P(\theta_r)$. The dihedral angle distribution function $P(\phi_r)$ describing the $\boldsymbol{k}$–$\boldsymbol{k}'$–$\boldsymbol{j}'$ correlation can be expanded in a Fourier series as

$$P(\phi_r)=\frac{1}{2\pi}\left(1+\sum_{\text{even},n\geq2}a_n\cos n\phi_r+\sum_{\text{odd},n\geq1}b_n\sin n\phi_r\right), \tag{2}$$

where

$$a_n=2\langle\cos n\phi_r\rangle,\quad b_n=2\langle\sin n\phi_r\rangle. \tag{3}$$

The fully correlated center of mass (CM) angular distribution $P(\omega_t,\omega_r)$ is written as

$$P(\omega_t,\omega_r)=\sum_{kq}\frac{2k+1}{4\pi}\frac{1}{\sigma}\frac{\mathrm{d}\sigma_{kq}}{\mathrm{d}\omega_t}C_{kq}(\theta_t,\theta_r), \tag{4}$$

where $C_{kq}(\theta_t,\theta_r)=\sqrt{4\pi/(2k+1)}Y_{kq}(\theta_t,\phi_r)$ is modified spherical harmonics, $(1/\sigma)(\mathrm{d}\sigma_{kq}/\mathrm{d}\omega_t)$ is a generalized polarization-dependent differential cross sections (PDDCSs) and yields

$$\frac{1}{\sigma}\frac{\mathrm{d}\sigma_{k0}}{\mathrm{d}\omega_t}=0, \tag{5}$$

when k is odd,

$$\frac{1}{\sigma}\frac{\mathrm{d}\sigma_{kq+}}{\mathrm{d}\omega_t}=\frac{1}{\sigma}\frac{\mathrm{d}\sigma_{kq}}{\mathrm{d}\omega_t}+\frac{1}{\sigma}\frac{\mathrm{d}\sigma_{k-q}}{\mathrm{d}\omega_t}=0, \tag{6}$$

when k is even, and q is odd or k is odd and q is even,

$$\frac{1}{\sigma}\frac{\mathrm{d}\sigma_{kq-}}{\mathrm{d}\omega_t}=\frac{1}{\sigma}\frac{\mathrm{d}\sigma_{kq}}{\mathrm{d}\omega_t}-\frac{1}{\sigma}\frac{\mathrm{d}\sigma_{k-q}}{\mathrm{d}\omega_t}=0, \tag{7}$$

when k is even, and q is even or k is odd and q is odd.

The PDDCS can be written as

$$\frac{1}{\sigma}\frac{\mathrm{d}\sigma_{kq\pm}}{\mathrm{d}\omega_t}=\sum_{k1}\frac{k_1}{4\pi}S^{k_1}_{kq\pm}C_{k_1q}(\theta_t,0), \tag{8}$$

where $S^{k_1}_{kq\pm}=\langle C_{k_1q}(\theta_t,0)C_{kq}(\theta_r,0)[(-1^q)\,\mathrm{e}^{\mathrm{i}q\xi\phi_r}\pm\mathrm{e}^{-\mathrm{i}q\phi_r}]\rangle$ is an expected value and the angular brackets denoting the averages over all the angles.

In the present study, we calculate $(2\pi/\sigma)(\mathrm{d}\sigma_{00}/\mathrm{d}\omega_t)$, $(2\pi/\sigma)(\mathrm{d}\sigma_{20}/\mathrm{d}\omega_t)$, $(2\pi/\sigma)(\mathrm{d}\sigma_{22+}/\mathrm{d}\omega_t)$, and $(2\pi/\sigma)(\mathrm{d}\sigma_{21-}/\mathrm{d}\omega_t)$, which are named $PDDCS_{00}$, $PDDCS_{20}$, $PDDCS_{22+}$, and $PDDCS_{21-}$ respectively, in the cases of $k=0$ and $k=2$.

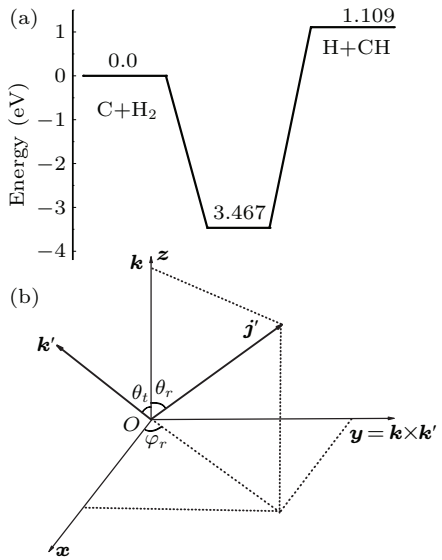


Fig. 1. (a) Schematic diagram of the PES for $C(^3P)+H_2(^1\Sigma_g^+) \rightarrow H(^2S)+CH(^2\Pi)$ reaction. (b) The $\boldsymbol{xyz}$ center-of-mass coordinate system used to describe the $\boldsymbol{k}$–$\boldsymbol{k}'$–$\boldsymbol{j}'$ correlations.

3. Results and discussion

3.1. Probability,integral cross sections, and rate constant

The reaction probabilities are calculated as a function of collision energy by employing QCT and QM methods for total angular momentum $J = 0$ displayed in Fig. 2(a). It is easily found that the reaction probability obtained by QM method presents a strong oscillation in the range of 1.0 eV–2.0 eV. It is mainly because of the property of the $CH_2(\tilde{X}\,^3A'')$ PES that has a deep potential well with the complex-forming mechanism. Overall, the reaction probability increases with the increase of collision energy, which is originated from that the $C(^3P)+H_2(^1\Sigma_g^+) \rightarrow H(^2S)+CH(^2\Pi)$ reaction is an endothermic reaction. It should be noted that in the range of 1.0 eV–1.1 eV, the collision energy is not big enough to cross the barrier of the system (greater than 1.1 eV), but the reaction probability is still not zero, which can be explained by the quantum tunneling effect. It is noteworthy that the inferiority of QCT reaction probabilities compared to the QM results enlarges with the increase of collision energy, from which we can conclude that the tunneling and zero-point energy effects cannot be ignored for the $C(^3P)+H_2(^1\Sigma_g^+) \rightarrow H(^2S)+CH(^2\Pi)$ reaction.

Figure 2(b) shows the ICSs in the collision energy range of 1.0 eV to 2.0 eV. The ICSs first increases rapidly and then moderately with a small fluctuation in the same collision range. Compared with the probability in the upper panel, the oscillation structures in the QM ICS curves are obviously weakened, caused by the J-average effect washing out the structures. Unlike the QM results, the ICSs calculated by QCT method show a least fluctuation and a most smoothness among the three methods. It can be indicated that the quantum effects caused resonances originated from the PES with the deeper potential well. We note that the ICSs calculated by QM method including the Coriolis coupling are always higher than the corresponding ICSs of CS in the entire collision energy range, and as the collision energy increases, the gap between the CS and CC ICSs is more obvious, indicating that the Coriolis coupling should not be ignored. Moreover, the QCT results are moderate among the three methods for collision energy bigger than 1.25 eV and become smallest for lower energy range. This significant discrepancies between QCT and CC methods are on account of the title reaction involving double H atoms causing obvious quantum effects. According to the above discussion, we can conclude that the QCT method is not appropriate for studying the ICSs and rate constants of the title reaction, which could provide theoretical support for the future study of this system.

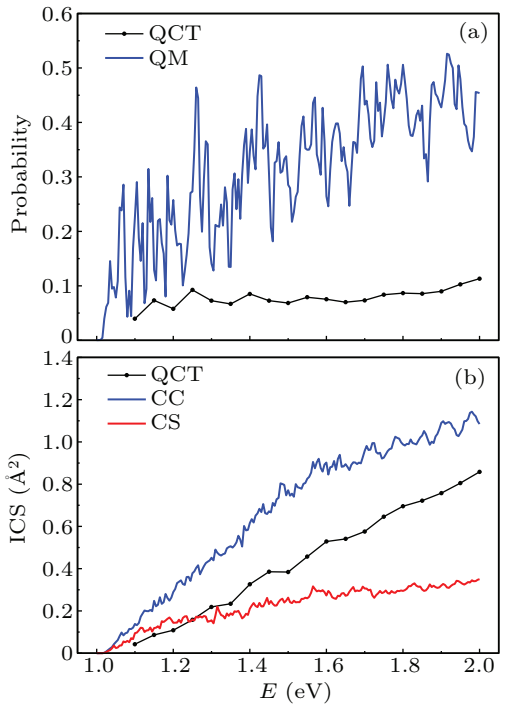


Fig. 2. The calculated reaction probability and ICS as a function of collision energy by employing QCT and QM methods.

Figure 3 indicates the CS and CC reaction probabilities for $C(^3P)+H_2(^1\Sigma_g^+) \rightarrow H(^2S)+CH(^2\Pi)$ reaction for $J = 5$, 10, 20, 30, 40, and 50 to explore the role of Coriolis coupling in this reaction with a deep well. Many sharp resonance peaks of probability appear because of the deep well on the $CH_2(\tilde{X}\,^3A'')$ PES. Both the CS and CC methods results increase with the increasing energy 1.0 eV–2.0 eV but decline with increasing J. The reactional thresholds arise and become larger as J rises. This indicates that the centrifugal barrier impedes the combination of C and H atoms. For $J = 5$, the CS probabilities are larger than CC probabilities, while for J being bigger than 5, the probabilities are reversed and the

dispersion between the two methods is more remarkable for larger J. It is owing to the reactant molecule, H_2, confined by just including $K_0 = 0$ quantum states in the CS approximation, which increases the opportunity for the sudden collision with C atom and then forms the product more easily with fewer resonances, resulting in overestimation of the reaction probability. With J increasing to a certain extent, much more partial waves contribute to the breaking of the collision complex through Coriolis coupling and thus facilitating the formation of the CH molecule. Consequently, when J becomes larger, the differences between the CS and CC probabilities are observed to be more and more remarkable, and in more details, the J-dependent behavior is observed that the CC probabilities tend to increase with increasing J. The above analysis shows that the Coriolis coupling effect is large and cannot be ignored.

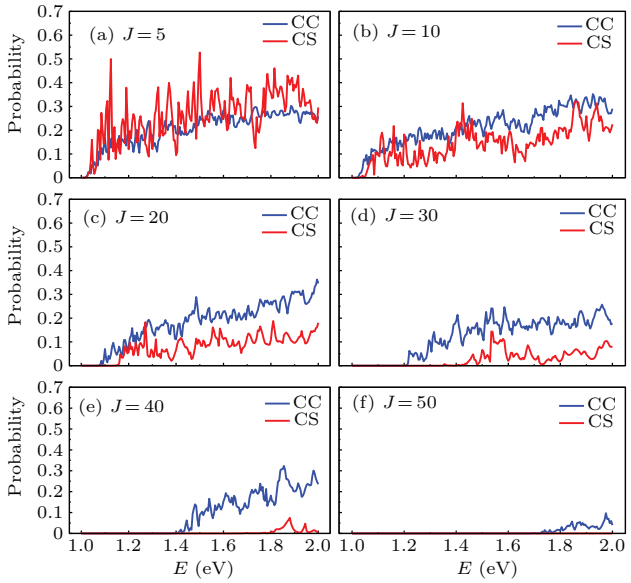


Fig. 3. Comparison between the CC and CS probabilities in the collision energy range of 1.0 eV to 2.0 eV for the total angular momentum (a) $J = 5$, (b) $J = 10$, (c) $J = 20$, (d) $J = 30$, (e) $J = 40$, and (f) $J = 50$.

In the temperature range from 1000 K to 2000 K, the rate constant of the $C(^3P) + H_2(^1\Sigma_g^+) \rightarrow H(^2S) + CH(^2\Pi)$ reaction is given in Fig. 4, obtained from the two different QM calculations. In calculations, the electronic population

$$f_{el}(T) = \frac{3}{3 \times \exp(-23.615/T) + 5 \times \exp(-62.426/T)} \quad (9)$$

is introduced. The two different QM calculations suggest the rate constant of CC calculations is stably higher than the corresponding CS method. Both the CC and CS results show the similar decline trend with the temperature reduced and the CC rate constant reduces among 10^{-16} cm^3/s to 10^{-13} cm^3/s from 1000 K to 2000 K. For the $C(^3P) + H_2(^1\Sigma_g^+) \rightarrow H(^2S) + CH(^2\Pi)$ reaction, it is obvious that the influence of Coriolis coupling on the title reaction is significant, and neglecting the Coriolis coupling for the title reaction is inappropriate.

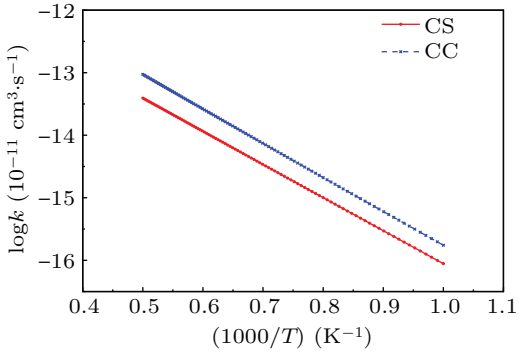


Fig. 4. Comparison between the CC and CS rate coefficients.

3.2. Stereodynamics

Because the trend of ICS calculated by QCT method is consistent with that by QM method, we can use QCT method to explore the stereodynamics information of the title reaction. Figure 5 shows the $\boldsymbol{k}$–$\boldsymbol{k}'$–$\boldsymbol{j}'$ correlation and the scattering direction of the product molecule CH for the $C(^3P) + H_2(^1\Sigma_g^+) \rightarrow H(^2S) + CH(^2\Pi)$ reaction according to the collision energy ranging from 1.0 eV to 2.0 eV described by the PDDCSs. Because the $PDDCS_{00}$ explains the $\boldsymbol{k}$–$\boldsymbol{k}'$ correlation and is just proportional to the differential cross section (DCS), it is easily found in panel (a) that the products are scattered both forward and backward. The larger the collision energy, the stronger the backward scattering. The reason for these results may be the PES has a deep potential well, and the indirect reaction mechanism dominates in the lower collision energy. And the complex in the indirect reaction has a long lifetime, so a symmetric product distribution can be easily formed. As the collision energy increases, the direct reaction mechanism begins to work. The shortened life of the complex leads to the partial forward or backward scattering, which gives the asymmetric distribution of DCS with the scattering angle. The panel (b) displays the $PDDCS_{20}$ of $(2\pi/\sigma)(d\sigma_{20}/d\omega_t)$, which is not only related to θ_t, but also a function of $\langle(3\cos^2\theta_r - 1)\rangle$. When the value of $\langle(3\cos^2\theta_r - 1)\rangle$ is negative, $\boldsymbol{j}'$ is strongly aligned perpendicular to $\boldsymbol{k}$ direction. The behavior of $PDDCS_{20}$ is opposite to that of $PDDCS_{00}$, and it is negative for both backwards and forwards scattered products, indicating that $\boldsymbol{j}'$ is preferentially aligned along the direction perpendicular to $\boldsymbol{k}$.

The PDDCSs with $q \neq 0$ are shown in panels (c) and (d). Because the $\boldsymbol{k}$–$\boldsymbol{k}'$ scattering plane is uncertain at the extreme of the scattering angle, so the values of PDDCSs are zero at $\theta = 0$ and $\theta = \pi$. Otherwise, the PDDCSs provide information about ϕ_r. And the values of PDDCSs are nonzero between 0 and π, this indicates that the $P(\theta_r, \phi_r)$ distribution is anisotropic for scattering products. The PDDCSs of $(2\pi/\sigma)(d\sigma_{22+}/d\omega_t)$ and $(2\pi/\sigma)(d\sigma_{21-}/d\omega_t)$ are respectively in connection with the $\langle(\sin^2\theta_r \cos 2\phi_r)\rangle$ and

$\langle(\sin 2\theta_r \cos\phi_r)\rangle$. When the PDDCS_{22+} is negative, product alignment is along the y axis, otherwise, the product alignment is along the x axis. And when the PDDCS_{21-} is negative, the product alignment is along the direction of the vector $\boldsymbol{x}+\boldsymbol{z}$, while the PDDCS_{21-} is positive means the product alignment along the direction of vector $\boldsymbol{x}-\boldsymbol{z}$. As shown in Fig. 5(c), the PDDCS_{21-} distribution is negative in most scattering angles, especially at $\theta_t = 140^\circ$ and $E_c = 1.2$ eV–1.6 eV, showing a clear product alignment along the y axis. While in panel (d), the value of the PDDCS_{21-} is clearly negative at $\theta_t = 160^\circ$ and $E_c = 1.7$ eV–1.9 eV, so the product alignment is along the direction of the vector $\boldsymbol{x}+\boldsymbol{z}$.

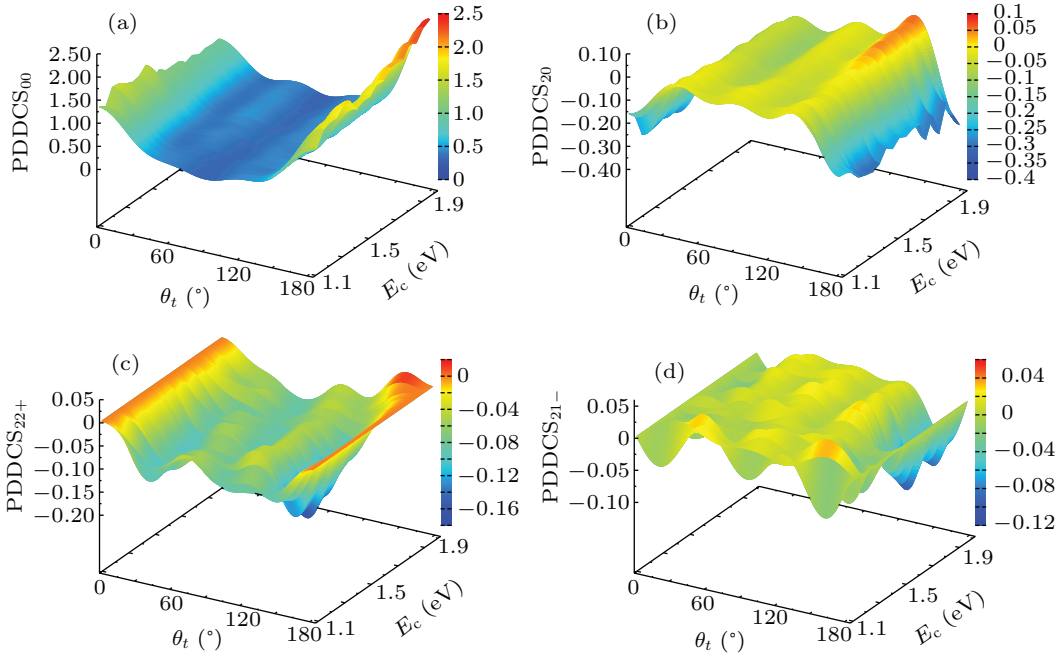


Fig. 5. The differential cross sections as functions of both the scattering angle θ_t over the range of 0°–180° and the collision energy over the range of 1.0 eV–2.0 eV.

The $P(\theta_r)$ distribution over the range of 0°–180° and energy covering the range of 1.1 eV–2.0 eV is described in Fig. 6. The distribution are symmetric about $\theta_r = 90^\circ$, and a 90° peak is obvious, which shows the rotational angular momentum alignment vertical to the reactant relative velocity and the remarkable polarization. Overall, there are a slight increase of $P(\theta_r)$ with increasing collision energy ranging from 1.0 eV–2.0 eV. The collision energy influences the $P(\theta_r)$ distribution positively and moderately.

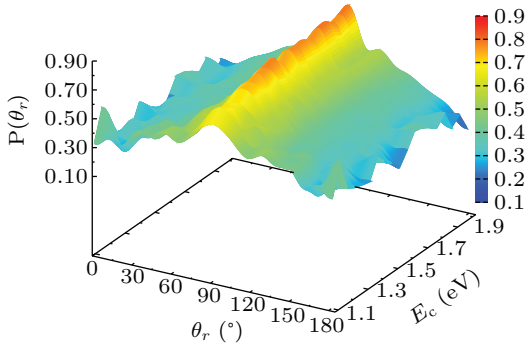


Fig. 6. The angular distribution of $P(\theta_r)$ replacing $\boldsymbol{k}$–$\boldsymbol{j}'$ correlation as functions of both angles of 0°–180° and the collision energy over the range of 1.0 eV–2.0 eV.

Figure 7 shows the dihedral angle distributions of $P(\phi_r)$ describing the $\boldsymbol{k}$–$\boldsymbol{k}'$–$\boldsymbol{j}'$ correlation at collision energies of 1.1, 1.2, 1.3, 1.4, 1.5, 1.6, 1.7, 1.8, 1.9, and 2.0 eV. In this figure we can find that the $P(\phi_r)$ is asymmetric with respect to the $\boldsymbol{k}$–$\boldsymbol{k}'$ scattering plane, and the peak at $\phi_r = 90^\circ$ is higher than at $\phi_r = 270^\circ$. The result indicates that the rotational angular momentum vector j' of the product molecule is not only aligned, but also strongly oriented along the positive y axis.

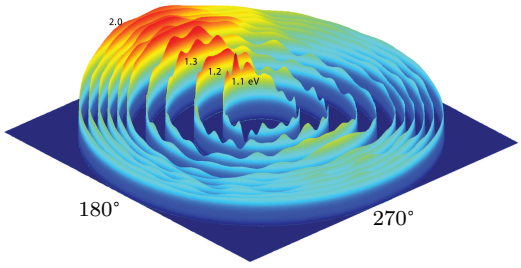


Fig. 7. The dihedral angle distributions of $P(\phi_r)$ describing the $\boldsymbol{k}$–$\boldsymbol{k}'$–$\boldsymbol{j}'$ correlation as functions of the dihedral angle ϕ_r at ten collision energies of 1.1, 1.2, 1.3, 1.4, 1.5, 1.6, 1.7, 1.8, 1.9, and 2.0 eV.

4. Conclusions

We have performed QM and QCT calculations for the $\mathrm{C}+\mathrm{H_2} \rightarrow \mathrm{H}+\mathrm{CH}$ reaction on the lowest triplet state $\mathrm{CH_2}(\tilde{X}\,^3A'')$ PES. The discrepancies between QM probabilities and QCT probabilities show that the tunneling and zero-point energy effects can not to be ignored for the reaction. The ICSs, probabilities and rate constants calculated by QM method including

the Coriolis coupling are always higher than the corresponding that of CS in the entire collision energy range, indicating values the Coriolis coupling should not be ignored. The calculated normalized PDDCS shows that the products are scattered both forward and backward, and the larger the collision energy, the stronger the backward scattering. The analysis of $P(\theta_r)$ and $P(\phi_r)$ distributions tells that the j' of the rotational angular momentum of product molecule is not only aligned vertical to the reactant relative velocity, but also strongly oriented along the positive y axis. The present work can provide theoretical support for choosing which method to study the system in the future.

Acknowledgements

Project supported by the National Natural Science Foundation of China (Grant Nos. 11904394 and 12004216) and the Natural Science Foundation of Shandong Province, China (Grant No. ZR2020QA064).

References

[1] Gaydon A G and Wolfhard H G 1979 *Flames-Their Structure, Radiation and Temperature*, 4th edn. (New York: Wiley)
[2] Magain P and Gillet D 1987 *Astrono. Astrophys.* **184** L5
[3] Duley W W and Williams D A 1984 *Interstellar Chemistry* (London: Academic Press)
[4] Becker K H, Engelhardt B, Wiesenk P and Bayes D 1989 *Chem. Phys. Lett.* **154** 342
[5] Dean A J, Davidson D F and Hanson R K 1991 *J. Phys. Chem.* **95** 183
[6] Beärda R A, van Hemert M C and van Dishoeck E F 1992 *J. Chem. Phys.* **97** 8240
[7] Scott D C, De Juan J, Robie D C, Schwartz-Lavi D and Reisler H 1992 *J. Phys. Chem.* **96** 2509
[8] Jursich G M and Wiesenfeld J R 1985 *J. Chem. Phys.* **83** 910
[9] Mikulecky K and Gericke K 1993 *J. Chem. Phys.* **98** 1244
[10] Blint R and Newton M 1975 *Chem. Phys. Lett.* **32** 178
[11] Joseph S and Varandas A J C 2009 *J. Phys. Chem. A* **113** 4175
[12] Knowles P J, Handy N C and Carter S 1983 *Mol. Phys.* **49** 681
[13] Harding L B 1983 *J. Phys. Chem.* **87** 441
[14] Bunker P R, Jensen P, Kraemer W P and Beardsworth R 1986 *J. Chem. Phys.* **85** 3724
[15] Jensen P and Bunker P R 1988 *J. Chem. Phys.* **89** 1327
[16] Comeau D C, Shavitt I, Jensen P and Bunker P R 1989 *J. Chem. Phys.* **90** 6491
[17] Harding L B, Guadagnini R and Schatz G C 1993 *J. Phys. Chem.* **97** 5472
[18] Yarkony D R 1996 *J. Chem. Phys.* **104** 2932
[19] Yarkony D R 1998 *J. Chem. Phys.* **109** 7047
[20] Bussery-Honvault B, Honvault P and Launay J 2001 *J. Chem. Phys.* **115** 10701
[21] Bussery-Honvault B, Julien J, Honvault P and Launay J 2005 *Phys. Chem. Chem. Phys.* **7** 1476
[22] Abdallah D B, Najar F, Jaidane N, Lakhdar Z B and Honvault P 2008 *Chem. Phys. Lett.* **456** 7
[23] Gamallo P, Defazio P, Akpinar S and Petrongolo C 2012 *J. Phys. Chem. A* **116** 8291
[24] Zhang L L, Liu D, Yue D G, Song Y Z and Meng Q T 2020 *J. Phys. B: At. Mol. Opt. Phys.* **53** 095202
[25] Banares L, Aoiz F, Vázquez S A, Ho T S and Rabitz H 2003 *Chem. Phys. Lett.* **374** 243
[26] Lu R F, Wang Y H and Deng K M 2013 *J. Comput. Chem.* **34** 1735
[27] Lin S Y and Guo H 2003 *J. Chem. Phys.* **119** 11602
[28] Lin S Y and Guo H 2004 *J. Phys. Chem. A.* **108** 2141
[29] Zhang C, Fu M, Shen Z, Ma H and Bian W 2014 *J. Chem. Phys.* **140** 234301
[30] Wu Y, Zhang C, Cao J and Bian W 2014 *J. Phys. Chem. A* **118** 4235
[31] Shen Z, Cao J and Bian W 2015 *J. Chem. Phys.* **142** 164309
[32] Shen Z T, Ma H T, Zhang C F, Fu M K, Wu Y N, Bian W S and Cao J W 2017 *Nat. Commun.* **8** 14094
[33] Sun Z P, Zhao W K and Yang C L 2017 *Int. J. Quantum Chem.* **117** e25431
[34] Zhang C F, Zheng Y J, Cao J W and Bian W S 2017 *RSC Adv.* **7** 34348
[35] González-Lezana T, Larrégaray P, Bonnet L, Wu Y and Bian W S 2018 *J. Chem. Phys.* **148** 234305
[36] van Harrevelt R, van Hemert M C and Schatz G C 2002 *J. Chem. Phys.* **116** 6002
[37] Liu D, Zhao J, Wang L F, Song Y Z, Meng Q T and Zhang L L 2020 *Chem. Phys. Lett.* **749** 137398
[38] Zhang D H and Zhang J Z H 1994 *J. Chem. Phys.* **101** 1146
[39] Varandas A J, Chu T S, Han K L and Caridade P J 2006 *Chem. Phys. Lett.* **421** 415
[40] Chu T S and Han K L 2005 *J. Phys. Chem. A* **109** 2050
[41] Zhang Y, Cao E, Gao S B, Huang X, Meng Q T and Song Y Z 2017 *Int. J. Quantum Chem.* **117** e25343
[42] Zhang J Y, Xu T, Ge Z W, Zhao J, Gao S B and Meng Q T 2020 *Chin. Phys. B* **29** 063101
[43] Zhao J, Xu T, Zhang L L and Wang L F 2020 *Chin. Phys. B* **29** 023105
[44] Han K L, Zheng X G, Sun B F, He G Z and Zhang R Q 1991 *Chem. Phys. Lett.* **181** 474
[45] Ju L P, Han K L and Zhang J Z H 2009 *J. Comput. Chem.* **30** 305
[46] Chu T S and Han K L 2008 *Phys. Chem. Chem. Phys.* **10** 2431
[47] Lin S Y, Han K L and Zhang J Z 2000 *Chem. Phys. Lett.* **324** 122
[48] Chu T S, Zhang Y and Han K L 2006 *Int. Rev. Phys. Chem.* **25** 201